Magnetic Shape Memory Polymers with Integrated Multifunctional Shape Manipulation

Qiji Ze, Xiao Kuang, Shuai Wu, Janet Wong, S. Macrae Montgomery, Rundong Zhang,
Joshua M. Kovitz, Fengyuan Yang, H. Jerry Qi,* and Ruike Zhao*

Shape-programmable soft materials that exhibit integrated multifunctional shape manipulations, including reprogrammable, untethered, fast, and reversible shape transformation and locking, are highly desirable for a plethora of applications, including soft robotics, morphing structures, and biomedical devices. Despite recent progress, it remains challenging to achieve multiple shape manipulations in one material system. Here, a novel magnetic shape memory polymer composite is reported to achieve this. The composite consists of two types of magnetic particles in an amorphous shape memory polymer matrix. The matrix softens via magnetic inductive heating of low-coercivity particles, and high-remanence particles with reprogrammable magnetization profiles drive the rapid and reversible shape change under actuation magnetic fields. Once cooled, the actuated shape can be locked. Additionally, varying the particle loadings for heating enables sequential actuation. The integrated multifunctional shape manipulations are further exploited for applications including soft magnetic grippers with large grabbing force, reconfigurable antennas, and sequential logic for computing.

Shape programmable soft materials that exhibit integrated multifunctional shape manipulations, including reprogrammable, untethered, fast, and reversible shape transformation and locking, in response to external stimuli, such as heat, light, or magnetic field,[1] are highly desirable for a plethora of applications, including soft robotics,[2] actuators,[3] deployable

Dr. Q. Ze, S. Wu, R. Zhang, Prof. R. Zhao
Department of Mechanical and Aerospace Engineering
The Ohio State University
Columbus, OH 43210, USA
E-mail: zhao.2885@osu.edu
Dr. X. Kuang, J. Wong, S. M. Montgomery, Prof. H. J. Qi
The George W. Woodruff School of Mechanical Engineering
Georgia Institute of Technology
Atlanta, GA 30332, USA
E-mail: qih@me.gatech.edu
Dr. J. M. Kovitz
Georgia Tech Research Institute
Atlanta, GA 30332, USA
Prof. F. Yang
Department of Physics
The Ohio State University
Columbus, OH 43210, USA

devices,[4] and biomedical devices.[2,5] A wide range of novel materials have been developed in the past, including liquid crystals elastomers,[6] hydrogels,[7] magnetic soft materials,[2,8] and shape memory polymers (SMPs).[1a,9] Despite these efforts, to date there is no single material system that can integrate multifunctional shape manipulations. Table S1 in the Supporting Information summarizes the shape manipulation capabilities of most shape programmable soft materials. One challenge in developing such a material system is that some of these shape manipulations are contradictory to each other. For example, fast reversibility requires rapid shape transformation by actuation but locking demands strong resistance to actuation.

Magnetic soft materials composed of magnetic particles in a soft polymer matrix have drawn great interest recently due to their untethered control for shape change,[10] motion,[2,3,11] and tunable mechanical properties.[12] Among them, hard-magnetic soft materials utilize high-remanence, high-coercivity magnetic particles, such as neodymium–iron–boron (NdFeB), to achieve complex programmable shape changes.[2,8,13] Under an actuation magnetic field, these particles with programmed domains exert micro-torques, leading to a large macroscopic shape change. However, the actuated shape cannot be locked as it needs a constantly applied magnetic field, which is energy inefficient. Additionally, these materials are very soft (with Young's modulus of about 1 MPa). In many practical applications, such as soft robotic grippers[14] and morphing antennas,[15] it is highly desirable that the actuated shape can be locked with high enough stiffness so that the material can fulfill certain functions requiring high supporting or self-supporting force without the constant presence of external stimulation.

SMPs can be programmed and fixed into a temporary shape and then recover the original shape under external stimuli, such as heat or light.[16] Typically, a thermally triggered SMP uses a transition temperature (T_{tran}), such as glass transition temperature (T_g), for the shape memory effect. In a shape memory cycle, an SMP is programmed to a temporary shape by an external force at a temperature above T_{tran} followed by cooling and unloading. The SMP recovers its original shape at temperatures above T_{tran} by direct heating or inductive heating.[17] However, conventional SMPs have the drawback of

**ADVANCED
SCIENCE NEWS**

www.advancedsciencenews.com
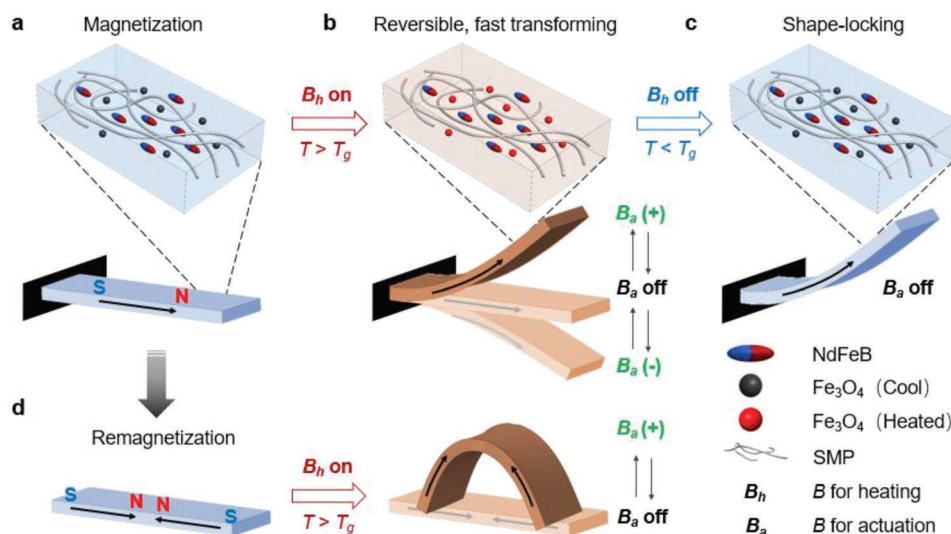
**ADVANCED
MATERIALS**

www.advmat.de

Figure 1. Working mechanism of magnetic shape memory polymers (M-SMPs). a) An M-SMP is stiff at low temperature and cannot be actuated by an applied actuation field (B_a). b) By applying a heating magnetic field (B_h), the M-SMP softens and can be actuated. c) Upon turning off B_h, the M-SMP is cooled and stiffens. Then the actuated shape is locked. d) The magnetization profile of the M-SMP can be reprogrammed to allow a different actuation.

one-way actuation. Although some recent efforts use crystallization/melting to achieve remarkable reversible and reprogrammable shape change, the actuation speed is limited by polymer crystallization/melting kinetics, which in general is relatively slow.[17b]

In this article, motivated by the advantages of hard-magnetic soft materials and SMPs, we report a novel M-SMP with integrated reprogrammable, untethered, fast, and reversible actuation and shape locking. The M-SMP is composed of two types of magnetic particles (Fe_3O_4 and NdFeB) in an amorphous SMP matrix. The Fe_3O_4 particles enable inductive heating under a high frequency alternating current (AC) magnetic field and thus are employed for shape locking and unlocking. The NdFeB particles are magnetized with predetermined magnetization profiles for programmable deformation under an actuation magnetic field. We demonstrate that the integrated multifunctional shape manipulations offered by M-SMPs can be exploited for a wide range of novel applications, including soft grippers for heavy loads, reconfigurable morphing antennas, and sequential logic circuits for digital computing.

Figure 1 shows the working mechanism of an M-SMP cantilever. Embedded with NdFeB and Fe_3O_4 particles, the M-SMP cantilever can be magnetized with a desired magnetic profile (e.g., along its longitudinal direction in Figure 1a) under an impulse magnetic field ($\approx$1.5 T). At room temperature, the cantilever is stiff and cannot deform under an actuation magnetic field (B_a). When a high frequency AC magnetic field (B_h) is applied (Figure 1b), the inductive heating of the Fe_3O_4 particles heats the M-SMP above its T_g, and the modulus of the M-SMP drops significantly. Then, a small B_a can easily bend the cantilever. By alternating B_a between up (+) and down (−) directions, fast transforming between upward and downward bending can be achieved. Upon removal of B_h (Figure 1c), the bending shape can be locked with high stiffness without further applying B_a once the temperature of the M-SMP drops below

its T_g. Moreover, the magnetization profile of the M-SMP can be reprogrammed for reconfigurable shape transformation by remagnetization. For example, remagnetizing the beam when it is mechanically locked in a folding shape will change the actuation to folding under the same B_a (Figure 1d).

To prove this concept, we fabricate an acrylate-based amorphous SMP with embedded NdFeB and Fe_3O_4 microparticles. For an M-SMP, it is essential to have a matrix SMP with a very low rubbery modulus so that, after adding NdFeB and Fe_3O_4 particles, the M-SMP can still have a relatively low modulus for actuation. Additionally, the neat SMP should have a large stretchability to allow large actuation. To balance the needs for high stretchability, low modulus, and tunable T_g, we design an SMP with an extremely low rubbery Young's modulus ($\approx$0.2 MPa) and mild T_g ($\approx$55 °C) with excellent mechanical properties (maximum stretch >200% at temperature between 25 to 85 °C) by rational selection of monomers and crosslinkers with a thermally induced free radical copolymerization approach. Our strategy is to use a low content of high molecular aliphatic urethane diacrylate cross-linker and rigid and flexible acrylate monomers. Widely tunable T_g can be achieved by adjusting the ratios of rigid and flexible acrylates (see the Experimental Section and Figures S1–S4 and Tables S2–S4 in the Supporting Information for more details). In addition, this resin can be photocured by using photoinitiators, which can be used for 3D printing in the future.

The neat SMP and M-SMP samples are prepared to characterize their thermomechanical and magnetic properties. **Figure 2**a–c shows the thermomechanical properties of the neat SMP and the M-SMP P15–15 (the two numbers represent the volume fractions of Fe_3O_4 and NdFeB particles, respectively). T_g, measured as the temperature at the peak of the tan δ curve, is $\approx$55 °C for the neat SMP, and $\approx$57 °C for P15–15 (Figure 2a). When the temperature T increases from 20 to 100 °C, the storage moduli of the neat SMP and P15–15 decrease from 1.3 and 2.9 GPa to 0.2 and 2.4 MPa, respectively. The high
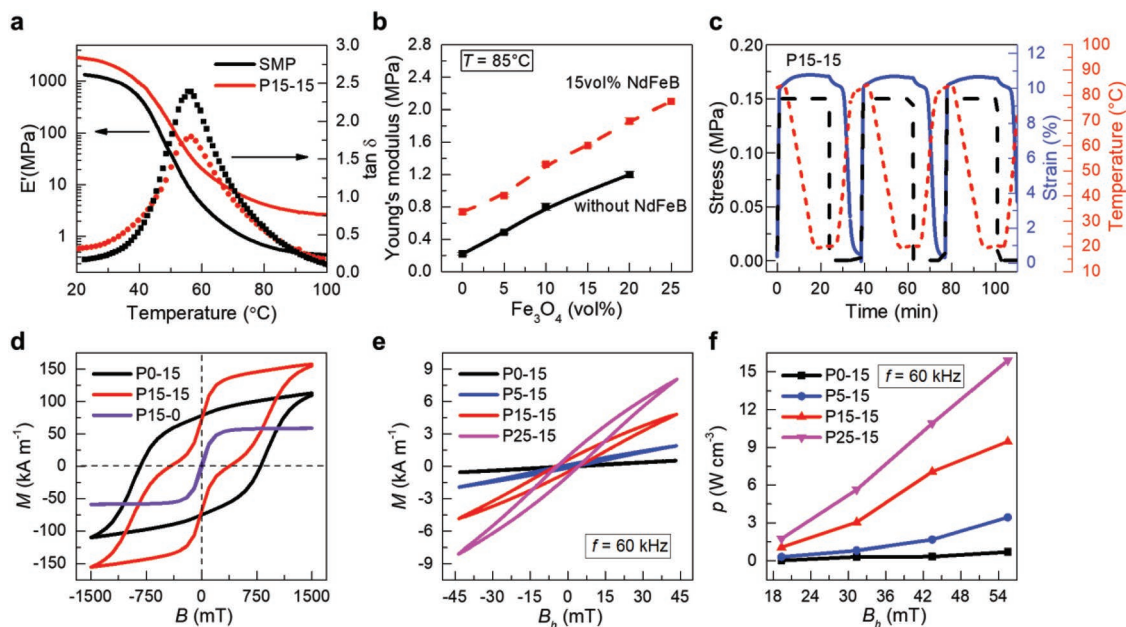
Figure 2. Thermomechanical and magnetic heating properties of M-SMPs. a) Storage modulus and tan δ versus temperature for the neat SMP and P15–15 (M-SMP with 15 vol% Fe_3O_4 and 15 vol% NdFeB). b) Effect of NdFeB and Fe_3O_4 particle loadings on Young's modulus of the M-SMPs at 85 °C. c) Shape memory performance of P15–15 in the 2nd to 4th cycles (black dashed line: stress; blue solid line: strain; red dashed line: temperature). d) Static magnetic hysteresis loops of the M-SMPs. M is the measured magnetic moment density under the applied magnetic field B. e) Hysteresis loops of the M-SMPs with different Fe_3O_4 loadings (P0–15, P5–15, P15–15, and P25–15) under 60 kHz AC magnetic field. f) Magnetic heating power density of the M-SMPs with different Fe_3O_4 loadings under different B_h.

modulus of M-SMPs at low temperature permits excellent capability for carrying heavy loads (see Figure S5 in the Supporting Information for additional information). The Young's modulus of the M-SMP at high-temperature increases linearly with increasing particle loading (Figure 2b), which allows easy tuning of the M-SMP properties for actuation. Figure 2c shows the strain, stress, and temperature as functions of time during the 2nd to 4th cycles of shape memory tests for P15–15. Due to the Mullins effect from high particle loading, the first cycle (Figure S6, Supporting Information) shows a relatively low shape recovery ratio. After the first cycle, the M-SMP shows stable shape memory performance. When P15–15 is programmed at 85 °C, it has the shape fixity and shape recovery ratios of ≈95% and ≈100%, respectively.

Figure 2d shows the static magnetic hysteresis loops of M-SMP P0–15 (NdFeB only), P15–0 (Fe_3O_4 only), and P15–15. Due to NdFeB's large remanence and coercivity, it can generate a magnetic torque for complex shape change under a small B_a. In contrast, Fe_3O_4's negligible magnetic hysteresis due to its low coercivity and low remanence makes it incapable of providing actuation force or heating power. However, under a high frequency AC magnetic field, the M-SMPs with Fe_3O_4 particles exhibit significantly increased magnetic hysteresis (Figure 2e, at 60 kHz AC field; Figure S7, Supporting Information), which allows them to be inductively heated by the hysteresis loss. We estimate the generated heating power by calculating the area of the hysteresis loop as shown in Figure 2f (see the Supporting Information for details). Increasing the loading of Fe_3O_4 particles or the strength of B_h will lead to a higher heating power. In this paper, the Fe_3O_4 particles with average size of 30 μm are selected to demonstrate the working mechanism of M-SMPs

after taking heating efficiency, material stiffness, and feasibility of fabrication into consideration (Figures S8 and S9, Supporting Information).[18] It should be mentioned that the low strength B_h (on the order of 10 mT) for inductive heating of Fe_3O_4 cannot heat up NdFeB as it would require much larger B_h (on the order of 1 T) due to NdFeB's huge coercivity. It should also be noted that the operating temperature should be limited to below 150 °C as NdFeB particles start to be demagnetized above this temperature (Figure S10, Supporting Information).

Here, we study the actuation of M-SMPs and demonstrate their remote fast transforming and shape locking can be used as soft robotic grippers. The experimental setup for M-SMP heating and actuation consists of two types of coils (**Figure 3**a): a pair of electromagnetic coils generate B_a for actuation; a solenoid provides B_h for inductive heating. It should be mentioned that it is possible to use one coil to apply both AC and DC fields for heating and actuation if a more sophisticated current wave control unit could be used. A P15–15 cantilever is fabricated with magnetization along its longitudinal direction so that the beam will tend to bend under a vertical magnetic field (Figure 3b). Here, we apply B_h = 40 mT at 60 kHz and B_a = 30 mT to heat and actuate the beam. The magnetic field profiles, as well as the measured cantilever displacement versus time, are shown in Figure 3c. The application of B_h gradually increases the temperature and the deflection of the M-SMP (Video S1, Supporting Information). We also alternate B_a at 0.25 Hz to show the reversible fast transforming. As shown in Figure 3b,c, the P15–15 beam gradually increases its deformation with the increasing temperature and reaches its maximum actuation at 23 s. The deformation at the rubbery state of the M-SMP can be well predicted by the finite element simulation
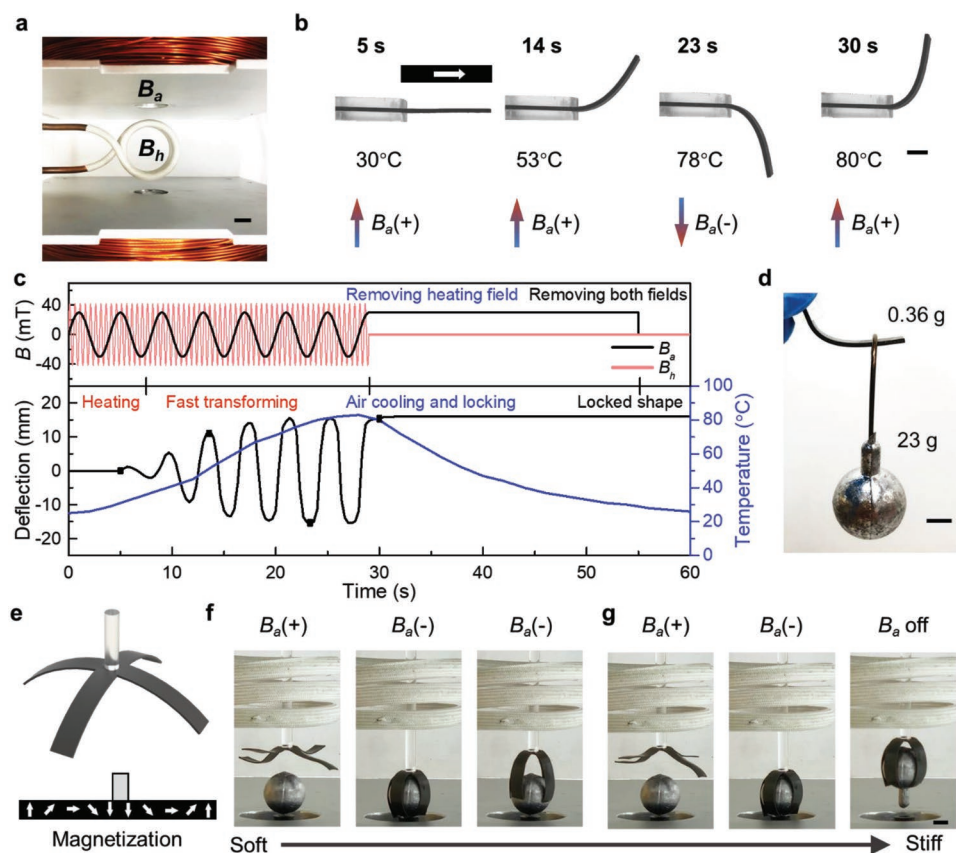
Figure 3. Fast-transforming and shape locking of M-SMPs via superimposed magnetic fields. a) Experimental setup for the superimposed magnetic fields: a pair of electromagnetic coils generates the actuation magnetic field, B_a; the solenoid in the middle generates the heating magnetic field, B_h. b) Cantilever bending and shape locking. c) Magnetic field profiles of B_a and B_h and beam deflection and temperature with respect to time. d) Locked bending beam carrying a weight (23 g) that is 64 times heavier than its weight (0.36 g). e) Design and magnetization profile of a four-arm M-SMP gripper (0.47 g). f,g) M-SMP gripper lifting a lead ball (23 g) without (f) and with (g) shape locking. Scale bars: (a): 15 mm; (b,d,g): 5 mm.

(Figure S11, Supporting Information).[13b] Upon removal of B_h at 29 s, the temperature decreases and the modulus of the M-SMP increases dramatically (Figure 2a). The bending shape can then be locked without further application of B_a. Figure 3d shows the M-SMP cantilever carrying a weight (23 g) that is 64 times heavier than its weight (0.36 g).

Soft robotic grippers are extensively researched due to their capability of adapting their morphology to grab objects. In general, it is highly desirable for a gripper to have untethered, reversible actuation with the capability of lifting or holding heavy objects without continuous energy assumption. Although active materials have been intensively explored in recent years, no single material can meet these highly desired merits. For example, the low-stiffness nature of soft materials significantly limits the actuation force, making most soft robotic grippers incapable of grabbing heavy objects. Conventional SMPs are also used as grippers, but due to lack of reversible actuation, their applications are limited. Taking M-SMPs' advantage of reversible actuation and shape locking, we demonstrate a soft robotic gripper that can grab heavy objects. Figure 3e shows the design and magnetization directions of a four-arm gripper (Figure S12, Supporting Information). By applying B_h and a positive B_a (upward), the gripper softens and opens up for grabbing. Upon switching B_a to negative, the gripper conforms to

the lead ball. At this moment, the ball slips if the gripper is lifted (Figure 3f). However, as demonstrated in Figure 3g, the gripper can be stiffened and locked into the actuated shape after we remove B_h. It can then effectively lift the lead ball without any external stimulation (Video S2, Supporting Information). The weight of the lead ball (23 g) is 49 times heavier than the gripper (0.47 g). Note that the lifting ratio (the ratio between the weights of the object and the gripper) can be significantly increased by decreasing the particle loading of NdFeB or/and Fe_3O_4, which may require a larger B_a or/and a larger or longer B_h for actuation and unlocking (see Table S5 in the Supporting Information for more information). With P3–3, we can achieve a lifting ratio of 1113, which is significantly higher than the reported soft grippers to date. Table S6 in the Supporting Information shows the comparison of the M-SMP-based gripper with other grippers reported in the literature. Additionally, the fast and reversible actuation of the M-SMP-based gripper permits multiple uses and reconfigurable grasping motions, which is advantageous compared with conventional SMP-based grippers that only allow a single grabbing operation.[19]

The ability to change the antenna shape on the fly provides the capability to either remotely deploy an antenna[20] or reconfigure its functionality.[21] In a morphing antenna, it is essential that the transformed shape can be locked so that the antenna can
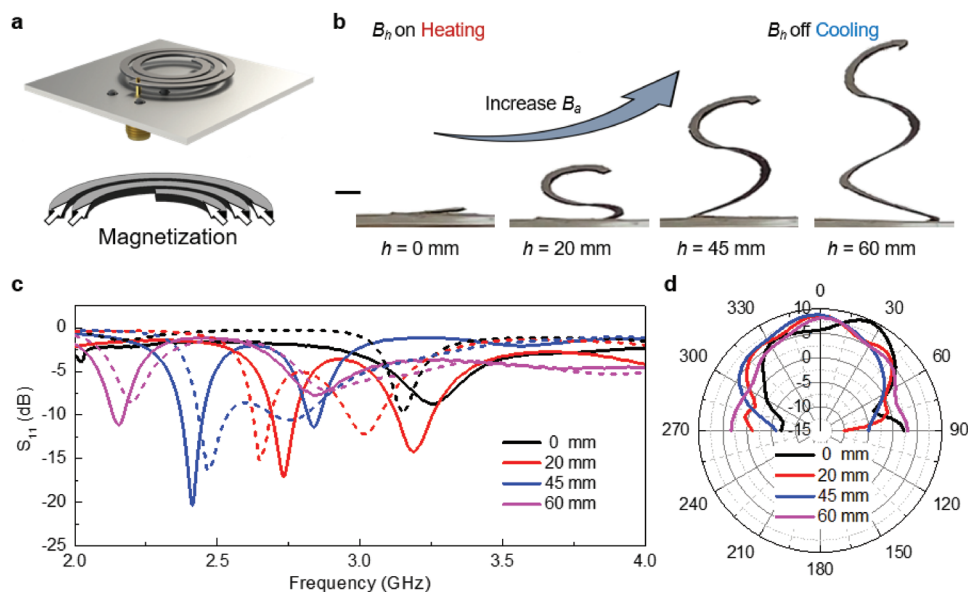
Figure 4. Application of M-SMPs for morphing antenna. a) Schematic and magnetization profile of a reconfigurable helical antenna. b) Actuation of the helical antenna under different B_a. c) Experimental (solid lines) and simulation (dashed lines) results of S_{11} band for the reconfigurable helical antenna at different heights. d) 2D polar plot of the simulated radiation patterns of the helical antenna at different heights. Scale bar in (b): 5 mm.

perform its function without consuming energy to maintain the actuated shape. Utilizing M-SMPs' advantages of shape transformation and locking, the on-demand shape transformation from a planar state to a 3D structure can also be achieved. Here we design a tapered helical antenna to achieve frequency reconfigurability. The antenna is composed of a thin M-SMP substrate with printed conductive silver wire on its surface (**Figure 4**a). The M-SMP substrate is magnetized in a stretched, spring-like configuration (Figure S13, Supporting Information) to realize the pop-up actuation with programmable heights and configurations under a controlled vertical B_a (Figure 4b; Video S3, Supporting Information). The simulation and experimental results in Figure 4c show that the resonant frequency of the antenna can be readily tuned between 2.15 and 3.26 GHz. The simulated radiation patterns at resonance with similar profiles shown in Figure 4d indicate that the operating direction of the antenna remains constant, which is desirable for antenna applications. Due to the shape locking capability offered by the M-SMP, the reconfigured antenna can retain the new shape without assistance from the external field, which lowers the overall energy requirements. Using M-SMPs as a substrate material for a remotely controlled, reconfigurable antenna is thus advantageous over the mechanically programmed antenna[15b] and conventional magnetic-responsive antenna.[22] A simple cantilever-based deployable and morphing antenna is also shown in Video S4 in the Supporting Information. There, the antenna achieves its transition from a deployable antenna to a reconfigurable one by reprogramming M-SMPs magnetization profile (Figure S14, Supporting Information), indicating the great flexibility and functionality of the M-SMP serving as a substrate material for flexible electronic devices.

The sequential shape transformation of an object in a predefined sequence can enable a material or system to fulfill multiple functions.[11,23] Here, we show that the sequential actuation of an M-SMP system can be achieved by designing

and actuating material regions with different Fe_3O_4 loadings for different resultant heating temperatures and stiffnesses under the same applied B_h. We prepare three M-SMPs with the same dimensions containing the same amount of NdFeB (15 vol%) but different amounts of Fe_3O_4 (5, 15, and 25 vol%, named as P5–15, P15–15, and P25–15, respectively). **Figure 5**a shows the mechanical and heating characterizations of the three M-SMPs under the same B_h (see the Experimental Section and Figure S15 in the Supporting Information). To reach the temperature (around 50 °C) at which the M-SMPs become reasonably soft to deform under B_a, it takes 5, 11, and 35 s for P25–15, P15–15, and P5–15, respectively.

Based on the mechanism of sequential actuation, we design a flower-like structure made of M-SMP petals using P5–15 and P25–15 to demonstrate the programmable sequential motion (Figure 5b). The P5–15 petals are designed to be longer than the P25–15 ones, and the magnetization is along the outward radial direction for all petals (Figure S16a, Supporting Information). Figure 5c shows the magnetic profiles and deflections (defined as the vertical displacements of the endpoints) of P5–15 and P25–15 petals as functions of time. The sequential shape change is illustrated in Figure 5d. Upon the application of B_h and a negative B_a, the P25–15 petals soften and start to bend first due to the large heating power. During this time, the P5–15 petals are heated slowly and remain straight because of their low temperature and high stiffness. With increasing heating time, the P5–15 petals start to soften and bend and are eventually fully actuated to lift the entire flower at 32 s. After removing B_h and cooling the flower down to room temperature, all petals are locked in their deformed shape. The fast transforming feature of M-SMPs is also demonstrated by switching the magnetic field direction during the actuation process (Video S5, Supporting Information). Video S6 and Figure S16b in the Supporting Information show a flower blooming-inspired sequential shape-transformation of an M-SMP system using P5–15, P15–15, and P25–15.
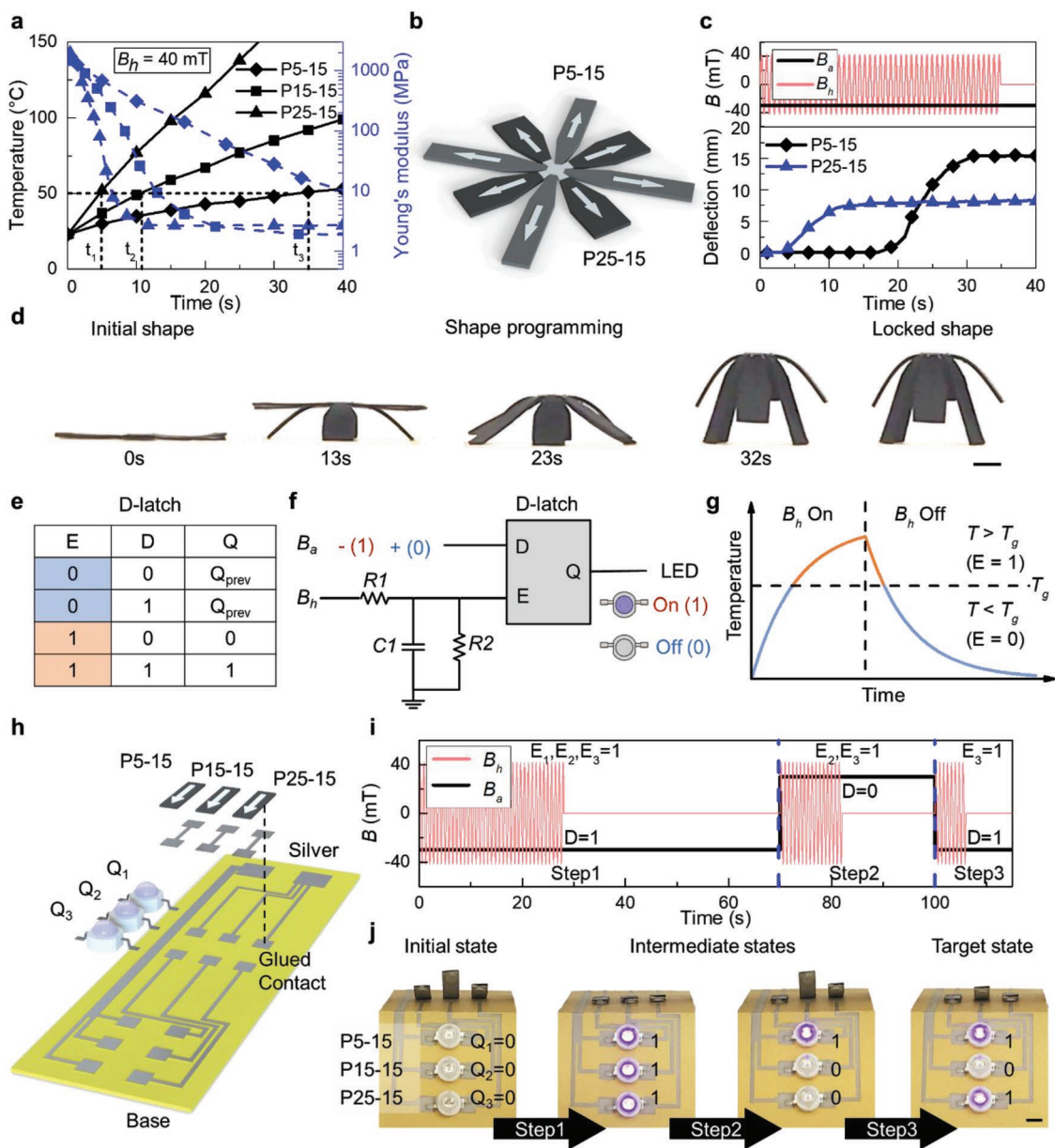
Figure 5. Sequential actuation of M-SMPs and their application as digital logic circuits. a) Temperature and corresponding Young's moduli of three M-SMPs containing different Fe_3O_4 loadings. b) Design and magnetization of a flower-like structure using P5–15 and P25–15. c) Magnetic field profiles (B_a and B_h) and deflection of the sequentially actuated M-SMPs with respect to time. d) Sequential shape transforming and shape locking. e) Truth table for a D-latch. f) Schematic of an M-SMP D-latch logic with two magnetic fields (B_a and B_h) serving as input and LED state as output. g) Relationship between B_h and the enabled input E of the D-latch. h) Design of the sequential logic circuit using M-SMPs with different Fe_3O_4 loadings (P5–15, P15–15, and P25–15). i) Magnetic control for the sequential logic circuit with three steps and outputs. j) LED indications for four different output states. Scale bars in (d) and (j): 5 mm.

Soft active materials and structures have recently been explored for programmable mechanical computing due to its capability of integrating actuation and computing in soft bodies for potential applications in the self-sensing of autonomous soft robots,[24] nonlinear dynamics-enabled unconventional computing,[25] and mechanical logic circuits.[26] Taking M-SMPs' advantages of reversible actuation and shape locking, we demonstrate that M-SMPs can be used to design a sequential logic device, the D-latch, for storing one bit of information, which can

be readily extended to a memory with arbitrary bits. The truth table for the D-latch logic is shown in Figure 5e: when the input E is 1, the output Q has the same value as the input D; when the input E is 0, the output Q stays latched and is independent of the input D. We achieve this D-latch logic utilizing the controlled actuation of an M-SMP beam switch (Figure 5f,g). The magnetic fields B_h and B_a work as inputs and the LED serves as the indicator of the output. The time-dependent actuation/locking of M-SMPs is interpreted as an RC delay circuit

**ADVANCED
SCIENCE NEWS**

www.advancedsciencenews.com

**ADVANCED
MATERIALS**

www.advmat.de

between B_h and the D-latch, where the heating/cooling time of the M-SMP is regarded as the charging/discharging time of a capacitor (Figure S17, Supporting Information). When B_h is on and the beam is unlocked ($T > T_g$, $E = 1$), the downward B_a ($D = 1$) or upward B_a ($D = 0$) determines whether the circuit is closed or open, leading to the on ($Q = 1$) or off ($Q = 0$) state of the LED. When B_h is off and the beam is locked ($T < T_g$, $E = 0$), B_a is no longer capable of actuating the beam and, consequently, cannot change the status of the LED. In other words, the previous state of Q is stored in the system.

With the M-SMP-enabled D-latch system, we next design a sequential digital logic circuit as a three-bit memory, which contains three M-SMP beams (P5–15, P15–15, and P25–15) and three LEDs shown in Figure 5h (see the Experimental Section and Figure S18 in the Supporting Information). Figure 5i shows the three-step logic for this three-bit memory, with E_1, E_2, and E_3 representing the input E for P5–15, P15–15, and P25–15, respectively. During the operation, heating for 28 s unlocks all M-SMPs (E_1, E_2, $E_3 = 1$), heating for 12 s unlocks P5–15 and P25–15 ($E_1 = 0$, E_2, $E_3 = 1$), and heating for 6 s only unlocks P25–15 (E_1, $E_2 = 0$, $E_3 = 1$). With the actuation (changing D) followed by cooling, the M-SMP switches can lock their shapes and retain the output status. Figure 5j shows the original state and output states for the three M-SMP switches indicated by the LEDs. In the first step, unlocking all M-SMPs (E_1, E_2, $E_3 = 1$) with $D = 1$ changes the memory state from 0–0–0 to 1–1–1. After cooling and locking (E_1, E_2, $E_3 = 0$), we next unlock P15–15 and P25–15 ($E_1 = 0$, E_2, $E_3 = 1$) and switch D to 0, which changes the memory state from 1–1–1 to 1–0–0. In the third step after full locking (E_1, E_2, $E_3 = 0$), we only unlock P25–15 (E_1, $E_2 = 0$, $E_3 = 1$) and switch D to 1 to finally change the memory state to 1–0–1 (Video S7, Supporting Information). This example demonstrates that by controlling the two inputs B_h (E) and B_a (D), we can erase and rewrite the information in the memory (Tables S7 and S8, Supporting Information). Theoretically, an electronic device with n-bit memory can be realized by n M-SMPs with varying particle loadings. In this way, $2n$ states can be achieved and stored with n steps by manipulating two inputs. Additionally, we can tune the NdFeB particle loading and T_g to provide more design flexibility for more complex computing systems using M-SMPs.

Although M-SMPs have many advantages, it should be noted that they also have some limitations. For example, the cooling speed for shape locking can be slow, which, however, is common for most heat-triggered soft active materials.[27] Also, a pair of electromagnetic coils is used to obtain a uniform magnetic field. But this may not be necessary in practical applications. For example, a solenoid or a permanent magnet can be used to provide effective heating or actuation, which can greatly simplify the setup.

In summary, the reported magnetic shape memory polymer integrates reprogrammable, untethered, fast, and reversible shape transformation and shape locking into one system. Utilizing two types of embedded magnetic particles for inductive heating and actuation, the material can be effectively unlocked and locked for energy-efficient operations in functions such as soft robotic grippers, deployable/reconfigurable antennas, sequential actuation devices, and digital logic circuits. With recent advances in simulation tools for design optimization

and 3D/4D printing for fabrication of complex structures, these demonstrations suggest that the novel M-SMP can serve as a material platform for a wide range of applications, including biomedical devices for minimally invasive surgery, active metamaterials, reconfigurable and flexible electronics, morphological computing, and autonomous soft robots.

Experimental Section

Preparation of the M-SMPs: In this work, the neat SMP is an acrylate-based amorphous polymer. The resin contains aliphatic urethane diacrylate (Ebecryl 8807, Allnex, Alpharetta, GA), 2-phenoxyethanol acrylate (Allnex), isobornyl acrylate (Sigma-Aldrich, St. Louis, MO, USA), and isodecyl acrylate (Sigma-Aldrich) with a weight ratio of 0.7:60.2:30.1:9. A thermal initiator (2,2′-azobis(2-methylpropionitrile), 0.4 wt%) is added for thermally induced free radical polymerization. Additionally, 2 wt% of fumed silica with an average size of 0.2–0.3 μm (Sigma-Aldrich) is added to ensure good mixing of the matrix resin with the magnetic particles. The composite is prepared by adding predetermined amounts of Fe_3O_4 (0–25 vol%) (particle size of 30 μm, Alpha Chemicals, MO, USA) and NdFeB magnetic particles (0–15 vol%) (average particle size of 25 μm, Magnequench, Singapore) in the matrix resin. Among the different materials used for inductive heating, such as iron oxides (Fe_2O_3 and Fe_3O_4), metals (cobalt and iron), and carbon nanotubes,[18,28] iron oxides are the most commonly used due to its high heating efficiency, chemical stability, and biocompatibility and are thus utilized here. The mixture is manually mixed, degassed under vacuum, and sandwiched between two glass slides for thermal curing. The spacing of the glass slides is varied depending on the application in which the magnetic film will be used. The thermal curing is conducted by precuring at 80 °C for 4 h and post-treatment at 120 °C for 0.5 h. The cured composite films are magnetized under impulse magnetic fields generated by an in-house built impulse magnetizer.

Electromagnetic Coil System for Actuation and Inductive Heating: A pair of in-house built electromagnetic coils with 74 mm spacing for actuating is used. The two coils are powered by a custom programmable power supply with up to 15 A output current. The coils can generate a central magnetic field at 7 mT A^{-1}. A water-cooled solenoid is connected to an LH-15A high-frequency induction heater to generate an AC magnetic field ranging from 10 to 60 mT at 60 kHz.

Physical Property Characterization: The uniaxial tension tests, dynamic thermomechanical properties measurements, and shape memory tests are conducted on a dynamic mechanical analysis (DMA) tester (DMA 850, TA Instruments, New Castle, DE) at various temperatures. The thin film samples (dimension: about 20 mm × 3 mm × 0.6 mm) are stretched at a strain rate of 0.2 min^{-1}. The strain is oscillated at a frequency of 1 Hz with a peak-to-peak amplitude of 0.1%. The temperature is ramped from 0 to 100 °C at the rate of 3 °C min^{-1}. The thermal imaging video (Video S1, Supporting Information) and temperature profiles (Figure 3c) are recorded using a thermal imaging camera. The dimension of the M-SMPs used for the temperature tests in Figure 5a and Figure S8c (Supporting Information) is 10 mm × 10 mm × 1 mm.

Cantilever Experiments: The M-SMP film is cut into a strip (35 mm × 4.5 mm). Two acrylic pieces (15 mm × 7 mm × 2 mm) are used to clamp one end of the M-SMP strip to create a cantilever with a length of 20 mm.

Gripper Experiments: Two M-SMP strips (47 mm × 5 mm × 0.5 mm) are cut and glued together to form a cross shape. The dimension of each arm is 21 mm × 5 mm. The four-arm gripper is softened and mechanically deformed to a grasping shape (diameter: 15 mm). The gripper is then cooled down and magnetized along the direction shown in Figure S12 (Supporting Information). After magnetization, a glass rod holder is glued to the central part of the gripper.

Sequential Logic Circuit Experiments: All beams used as switches in the sequential logic circuit have a dimension of 20 mm × 5 mm × 0.8 mm. Each beam is fixed at one end to the printed circuit. Silver paste (Dupont

ME603) is uniformly painted on the bottom surface of the beams and cured at 80 °C for 20 min. The LED leads, the fixed end of beams, and the copper wires for connecting the power supply are all attached to the printed circuit using silver paste. Finally, the assembled circuit is cured at 80 °C for another 20 min.

Supporting Information

Supporting Information is available from the Wiley Online Library or from the author.

Conflict of Interest

The authors declare no conflict of interest.

[1] a) A. Lendlein, S. Kelch, *Angew. Chem., Int. Ed.* **2002**, *41*, 2034; b) S.-J. Jeon, A. W. Hauser, R. C. Hayward, *Acc. Chem. Res.* **2017**, *50*, 161; c) Y. Liu, J. Genzer, M. D. Dickey, *Prog. Polym. Sci.* **2016**, *52*, 79; d) U. S. Jascha, F. Hortense Le, E. Paolo, R. S. André, F. A. Andres, *Bioinspiration Biomimetics* **2017**, *12*, 026012; e) R. M. Erb, J. S. Sander, R. Grisch, A. R. Studart, *Nat. Commun.* **2013**, *4*, 1712.

[2] W. Hu, G. Z. Lum, M. Mastrangeli, M. Sitti, *Nature* **2018**, *554*, 81.

[3] a) H.-W. Huang, M. S. Sakar, A. J. Petruska, S. Pané, B. J. Nelson, *Nat. Commun.* **2016**, *7*, 12263; b) J. Yuan, W. Neri, C. Zakri, P. Merzeau, K. Kratz, A. Lendlein, P. Poulin, *Science* **2019**, *365*, 155; c) Y.-F. Zhang, N. Zhang, H. Hingorani, N. Ding, D. Wang, C. Yuan, B. Zhang, G. Gu, Q. Ge, *Adv. Funct. Mater.* **2019**, *29*, 1806698.

[4] a) S. Felton, M. Tolley, E. Demaine, D. Rus, R. Wood, *Science* **2014**, *345*, 644; b) J. A. Faber, A. F. Arrieta, A. R. Studart, *Science* **2018**, *359*, 1386.

[5] a) J. Qin, I. Asempah, S. Laurent, A. Fornara, R. N. Muller, M. Muhammed, *Adv. Mater.* **2009**, *21*, 1354; b) K. Kobayashi, C. Yoon, S. H. Oh, J. V. Pagaduan, D. H. Gracias, *ACS Appl. Mater. Interfaces* **2019**, *11*, 151; c) Z. Hosseinidoust, B. Mostaghaci, O. Yasa, B.-W. Park, A. V. Singh, M. Sitti, *Adv. Drug Delivery Rev.* **2016**, *106*, 27; d) B. Mostaghaci, O. Yasa, J. Zhuang, M. Sitti, *Adv. Sci.* **2017**, *4*, 1700058.

[6] a) T. H. Ware, M. E. McConney, J. J. Wie, V. P. Tondiglia, T. J. White, *Science* **2015**, *347*, 982; b) B. R. Donovan, V. M. Matavulj, S.-k. Ahn, T. Guin, T. J. White, *Adv. Mater.* **2019**, *31*, 1805750.

[7] A. Sydney Gladman, E. A. Matsumoto, R. G. Nuzzo, L. Mahadevan, J. A. Lewis, *Nat. Mater.* **2016**, *15*, 413.

[8] Y. Kim, H. Yuk, R. Zhao, S. A. Chester, X. Zhao, *Nature* **2018**, *558*, 274.

[9] a) T. Xie, *Nature* **2010**, *464*, 267; b) J. L. Hu, Y. Zhu, H. H. Huang, J. Lu, *Prog. Polym. Sci.* **2012**, *37*, 1720; c) H. Meng, G. Q. Li, *Polymer* **2013**, *54*, 2199.

[10] a) J. Kim, S. E. Chung, S.-E. Choi, H. Lee, J. Kim, S. Kwon, *Nat. Mater.* **2011**, *10*, 747; b) V. Q. Nguyen, A. S. Ahmed, R. V. Ramanujan, *Adv. Mater.* **2012**, *24*, 4041.

[11] J. A.-C. Liu, J. H. Gillen, S. R. Mishra, B. A. Evans, J. B. Tracy, *Sci. Adv.* **2019**, *5*, eaaw2897.

[12] J. A. Jackson, M. C. Messner, N. A. Dudukovic, W. L. Smith, L. Bekker, B. Moran, A. M. Golobic, A. J. Pascall, E. B. Duoss, K. J. Loh, C. M. Spadaccini, *Sci. Adv.* **2018**, *4*, eaau6419.

[13] a) G. Z. Lum, Z. Ye, X. Dong, H. Marvi, O. Erin, W. Hu, M. Sitti, *Proc. Natl. Acad. Sci. USA* **2016**, *113*, E6007; b) R. Zhao, Y. Kim, S. A. Chester, P. Sharma, X. Zhao, *J. Mech. Phys. Solids* **2019**, *124*, 244; c) T. Xu, J. Zhang, M. Salehizadeh, O. Onaizah, E. Diller, *Sci. Rob.* **2019**, *4*, eaav4494; d) S. Wu, Q. Ze, R. Zhang, N. Hu, Y. Cheng, F. Yang, R. Zhao, *ACS Appl. Mater. Interfaces* **2019**, *11*, 41649.

[14] a) T. Wallin, J. Pikul, R. Shepherd, *Nat. Rev. Mater.* **2018**, *3*, 84; b) J. Shintake, V. Cacucciolo, D. Floreano, H. Shea, *Adv. Mater.* **2018**, *30*, 1707035.

[15] a) R. Al-Dahleh, C. Shafai, L. Shafai, *Microwave Opt. Technol. Lett.* **2004**, *43*, 64; b) H. Fu, K. Nan, W. Bai, W. Huang, K. Bai, L. Lu, C. Zhou, Y. Liu, F. Liu, J. Wang, *Nat. Mater.* **2018**, *17*, 268.

[16] a) Q. Zhao, H. J. Qi, T. Xie, *Prog. Polym. Sci.* **2015**, *49–50*, 79; b) A. Lendlein, O. E. C. Gould, *Nat. Rev. Mater.* **2019**, *4*, 116.

[17] a) U. N. Kumar, K. Kratz, M. Heuchel, M. Behl, A. Lendlein, *Adv. Mater.* **2011**, *23*, 4157; b) L. Wang, M. Y. Razzaq, T. Rudolph, M. Heuchel, U. Nöchel, U. Mansfeld, Y. Jiang, O. E. Gould, M. Behl, K. Kratz, *Mater. Horiz.* **2018**, *5*, 861.

[18] R. Hergt, S. Dutz, R. Müller, M. Zeisberger, *J. Phys.: Condens. Matter* **2006**, *18*, S2919.

[19] A. M. Hubbard, R. W. Mailen, M. A. Zikry, M. D. Dickey, J. Genzer, *Soft Matter* **2017**, *13*, 2299.

[20] a) S. Yao, X. Liu, J. Gibson, S. V. Georgakopoulos, in *2015 IEEE Int. Symposium on Antennas and Propagation & USNC/URSI National Radio Science Meeting*, IEEE, Piscataway, NJ, USA **2015**, pp. 2215–2216; b) J. Costantine, Y. Tawk, C. G. Christodoulou, J. Banik, S. Lane, *IEEE Antennas Wireless Propag. Lett.* **2012**, *11*, 285.

[21] a) J. M. Kovitz, H. Rajagopalan, Y. Rahmat-Samii, *IEEE Trans. Antennas Propag.* **2015**, *63*, 2497; b) G. Oliveri, D. H. Werner, A. Massa, *Proc. IEEE* **2015**, *103*, 1034; c) J. T. Bernhard, *Synth. Lect. Antennas* **2007**, *2*, 1.

[22] J.-C. Langer, J. Zou, C. Liu, J. T. Bernhard, *IEEE Microwave Wireless Compon. Lett.* **2003**, *13*, 120.

[23] Y. Liu, B. Shaw, M. D. Dickey, J. Genzer, *Sci. Adv.* **2017**, *3*, e1602417.

[24] a) P. Polygerinos, N. Correll, S. A. Morin, B. Mosadegh, C. D. Onal, K. Petersen, M. Cianchetti, M. T. Tolley, R. F. Shepherd, *Adv. Eng. Mater.* **2017**, *19*, 1700016; b) B. E. Treml, R. N. McKenzie, P. Buskohl, D. Wang, M. Kuhn, L. S. Tan, R. A. Vaia, *Adv. Mater.* **2018**, *30*, 1705616.

[25] K. Nakajima, H. Hauser, T. Li, R. Pfeifer, *Soft Rob.* **2018**, *5*, 339.

[26] a) N. S. G. K. Devaraju, M. A. Unger, *Lab Chip* **2012**, *12*, 4809; b) B. Treml, A. Gillman, P. Buskohl, R. Vaia, *Proc. Natl. Acad. Sci. USA* **2018**, *115*, 6916; c) D. J. Preston, P. Rothemund, H. J. Jiang, M. P. Nemitz, J. Rawson, Z. Suo, G. M. Whitesides, *Proc. Natl. Acad. Sci. USA* **2019**, *116*, 7750.

[27] M. J. Ford, C. P. Ambulo, T. A. Kent, E. J. Markvicka, C. Pan, J. Malen, T. H. Ware, C. Majidi, *Proc. Natl. Acad. Sci. USA* **2019**, *116*, 21438.

[28] Z. He, N. Satarkar, T. Xie, Y. T. Cheng, J. Z. Hilt, *Adv. Mater.* **2011**, *23*, 3192.